Pergamon

Int. J. Solids Structures Vol. 34, Nos. 35–36, pp. 4581–4596, 1997

0020–7683/97 $17.00 + .00

PII: S0020–7683(97)00041–3

PERFORATION OF STEEL AND POLYCARBONATE PLATES BY TUMBLING PROJECTILES

KEZHUN LI† and WERNER GOLDSMITH
Department of Mechanical Engineering, University of California, Berkeley, CA 94720, U.S.A.

(*Received* 3 *September* 1996; *in revised form* 20 *December* 1996)

Abstract—An experimental investigation to assess the effect of tumbling by hard-steel, blunt-faced cylindrical projectiles on the impact response of thin 4130 steel and polycarbonate target plates was performed. Deformation and failure phenomena were observed and discussed; comparisons of the results with analytical models and numerical stimulation, described in a previous paper, were also performed for the steel targets. The final velocity of the projectile and the crater length in the target were correlated with the striker impact angle (or yaw angle with a zero oblique angle); reasonable agreement was attained among the experimental, analytical and numerical results. It was found that an increase of the impact angle can increase the velocity drop and the crater length markedly. The increase tends to be stabilized after the impact angle exceeds 50° and the consequences in such a case are almost the same as in side-on impact. © 1997 Elsevier Science Ltd.

INTRODUCTION

Recent experimental, analytical and numerical studies of tumbling impact have been conducted by Li and Goldsmith (1995), (1996a), (1996b) and (1996c) that have focused on thin and moderately thick aluminum plates. It should be noted that tumbling impact incorporates yawing, oblique and rotational motion and represents a combination of several collision scenarios. The geometry and nomenclature for oblique impact without yaw, yawing impact without obliquity and the general case of impact with yaw and obliquity are reproduced from Li and Goldsmith (1996a) in Figs 1(a–c). The YAW angle, α, is defined as the angle between the longitudinal axis of the projectile and the velocity vector of the striker's center of mass. The OBLIQUE angle, β is the angle between the velocity vector and the target normal. The IMPACT (or trajectory) angle, Θ, is the angle between the projectile axis and the normal to the target so that $\Theta = a-\beta$ or $\Theta = \beta-\alpha$ depending on the relative orientation of the velocity vector **v**, the centerline and the target normal. Clearly, the impact angle equals the yaw angle when the oblique angle is zero. Terms v_o, v_f and ω_o and ω_f are the initial and final translational and rotational speeds of the striker.

Excellent agreement was obtained among the experimental, analytical and numerical results for both thin and moderately thick aluminum plates (Li and Goldsmith, 1966a, 1966b and 1966c). It was found from these studies that the impact angle plays a significant role in the perforation process. It can not only increase the velocity drop and decrease the ballistic limit, but also change the trajectory of the striker significantly, especially for thick targets, as determined by Li and Goldsmith (1996c). An increase in the initial velocity will decrease the percentage of the velocity drop and the change in the trajectory. The crater length of a target subject to an impact by a tumbling striker is substantially larger than that generated by normal perforation.

This paper presents the results of an investigation of tumbling impact on 3.2 and 1.6 mm thick 4130 steel and 6.4 and 3.2 mm thick polycarbonate plates with a 140 mm diameter, clamped on a 127 mm diameter in a rigid steel frame. Deformation patterns and failure modes of the targets were determined from examination of the photographs and the perforated specimens. Because of the similarity in the behavior of the steel and aluminum targets, the analytical model developed for the thin aluminum plates by Li and Goldsmith (1996b) was also employed for steel. The experimental results validate and a numerical simulation further supports the analytical model by good correspondence upon comparing

† Current Address: Case Corporation, 7 South 600 County Line Road, Burr Ridge, IL 60521, U.S.A.

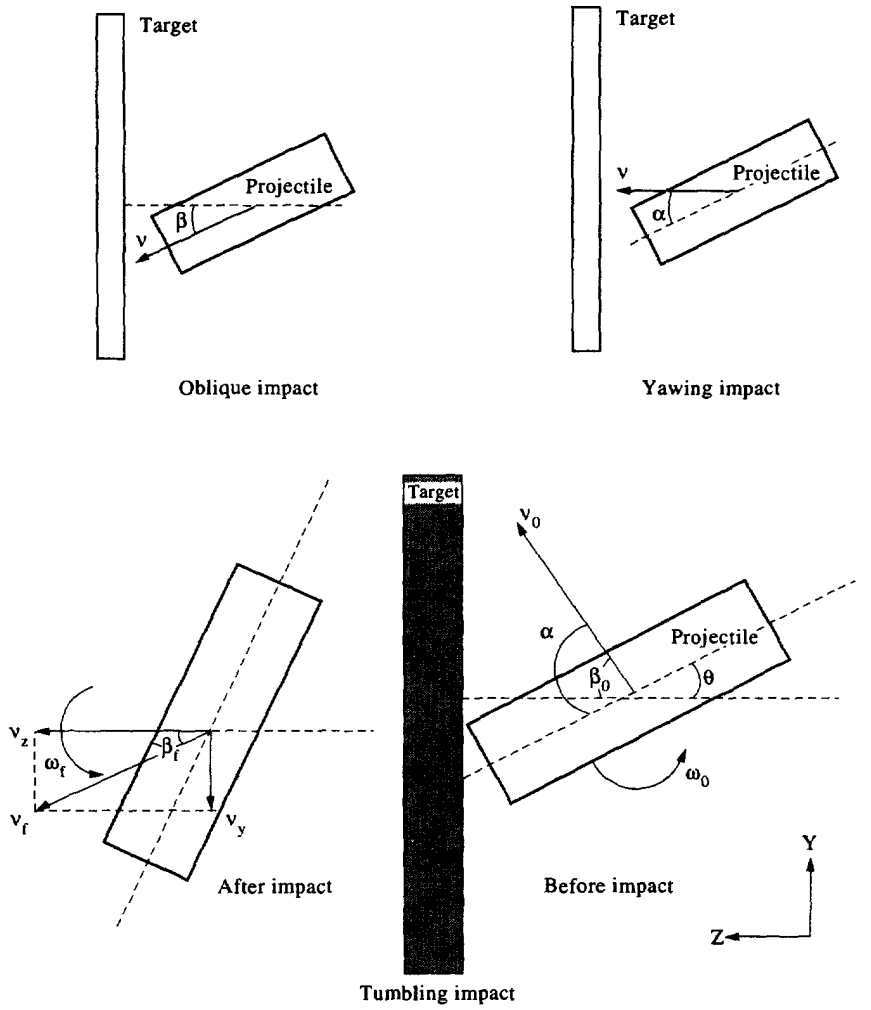

Fig. 1. Projectile impact: (a) at obliquity β without yaw; (b) with yaw α without obliquity; (c) with tumbling involving both yaw and obliquity.

both the final results and the details of the perforation process. However, polycarbonate targets manifest quite different phenomena from those of ductile metals such as steel and aluminum, and the analytical procedures employed for aluminum and steel, hence, could not be utilized for this plastic substance.

EXPERIMENTAL STUDY

The experimental technique producing tumbling of projectiles and a subsequent specified impact angle are described by Li (1994) and Li and Goldsmith (1966a). Tumbling was generated by overlapping contact of the high-speed blunt-faced cylindrical projectile with a 2024-0 or 6061-T6 aluminum block with dimensions of $102 \times 102 \times 25.4$ mm placed between the gun and the target plate. All data: initial and final velocities, impact angle, initial and final oblique angles as well as the rotational striker speed were obtained from high-speed photography. The initial projectile velocity was also monitored by the signals generated upon the interruption by the striker of two parallel laser beams passing through opposite slits in the gun and focused on photodiodes connected to an oscilloscope. The cylindrical projectiles, made of S-7 air hardened drill rod (R_C 54), had a diameter of 12.7 mm and a length of 38.1 mm. The material properties of the striker, obtained from the

Table 1. Properties of projectile and target material

Material	Density (kg m^{-3})	Dynamic yield stress (MPa)	Ultimate shear strength (MPa)	Ultimate tensile strain (%)
Projectile	7977	1393	804	—
Steel 4130	7700	560	323	28

Metals Handbook (1978) are listed in Table 1. In the present study, the velocities of the projectiles ranged from 250 to 700 m s^{-1}; impact angles varied from 0 to 65°; initial oblique angles spanned values from 0 to 18° and rotational speeds spanned values from 0 to 3000 rad s^{-1}. It was found by Li (1994) that the initial rotational speed prior to impact had little effect on the perforation process within the range of parameters investigated here. However, the major role of the rotation is to change the impact angle at contact and this will significantly affect the perforation event.

Table 2 presents the experimental results for tumbling perforation of 4130 steel and polycarbonate plates.

Seventeen shots were fired against 4130 steel plates, 11 on 3.2 mm thick and 6 on 1.6 mm thick samples. Photographic examination indicated no translational motion of the target, although bending was produced, as expected. When the impact angle was less than 50°, nearly cylindrical plugs were generated, as occurred in runs ST-14, Fig. 2 and ST-8, Fig. 3. Two possible failure modes, hole enlargement and front petaling (Wu and Goldsmith, 1990) ensued after plugging, due to the contact between the projectile lateral surface and the upper edge of the hole that were noted in the metal plates. Li (1994) and Li and Goldsmith (1996a) found that the impact angle played a dominant role in determining the failure phenomenon for a given target thickness. When the impact angle is small, hole

Table 2. Experimental results of perforation of plates by tumbling cylindrical projectiles

	Initial conditions					Final results			
Run	Target thickness (mm)	Velocity (m s^{-1})	Impact angle (deg)	Oblique angle (deg)	Angular velocity (rad/s)	Velocity (m s^{-1})	Oblique angle (deg)	Angular velocity rad/s)	Crater length (mm)
ST-1	3.2	612	1	6	970	*	*	*	22
ST-2	3.2	427	20	8	986	371	−1	912	34
ST-3	3.2	459	22	7	1031	400	−1	1017	33
ST-4	3.2	365	40	10	1679	282	5	2100	42
ST-5	3.2	626	3	4	1069	*	*	*	21
ST-6	3.2	461	32	8	1615	368	3	1617	37
ST-7	3.2	482	27	7	1313	410	−1	1152	35
ST-8	3.2	436	34	8	1596	367	1	1655	39
ST-9	3.2	418	51	10	2754	314	9	2558	41
ST-10	3.2	703	0	0	0	650	0	0	14
ST-11	3.2	570	0	0	0	526	0	0	14
ST-12	1.6	627	14	3	1873	581	2	1926	27
ST-13	1.6	554	16	5	1494	498	1	623	28
ST-14	1.6	570	13	4	819	537	1	2310	25
ST-15	1.6	300	63	17	3012	264	16	3104	40
ST-16	1.6	686	0	0	0	655	0	0	14
ST-17	1.6	556	0	0	0	530	0	0	14
PL-1	6.4	334	47	7	1383	*	*	*	34
PL-2	6.4	563	0	0	0	543	0	0	9
PL-3	6.4	700	0	0	0	679	0	0	11
PL-4	6.4	438	0	0	0	421	0	0	11
PL-5	6.4	261	0	0	0	242	0	0	12
PL-6	3.2	271	37	12	1061	235	12	697	27
PL-7	3.2	259	34	14	1129	*	*	*	22
PL-8	3.2	557	0	0	0	551	0	0	12
PL-9	3.2	690	0	0	0	685	0	0	12
PL-10	3.2	438	0	0	0	431	0	0	12

*: film not clear.

enlargement ensued after plugging, which resulted in slight thickening of the hole edge. With an increase of the impact angle, the failure mode tended to change from hole enlargement to front petaling. Here, two major cracks initiated from the upper portion of the projectile/target interface at both impact and distal sides and propagated outwards, as shown in Figs 2 and 3. The petal width approximated the projectile diameter; the petal was bent for a smaller impact angle (13°), as indicated in Fig. 2. For a relatively large impact angle (34°), the upper petal was punched out of the target, as displayed in Fig. 3. The critical impact angle representing transition from hole enlargement to front petaling was found by Li (1994) to be 8° for the 3.2 mm thick plate and 4° for the 1.6 mm thick target. When the impact angle was above 50°, the failure tended to be a tearing fracture and no circular plug was formed. Instead, only a single rectangularly-shaped plate component was detached from the target, as illustrated for run ST-15 in Fig. 4 where the impact angle was 63°.

Five perforation tests were performed on 6.4 mm thick plates of polycarbonate and five others on such targets with a thickness of 3.2 mm. In normal perforations or for relatively small impact angles, nearly circular plugs were produced. The hole exhibits a much smaller diameter than the projectile, evidencing substantial recovery. When the impact angle is large, an additional failure was invoked due to the oblique position of the projectile which results in contact between the lateral surface of the striker and the target. Two petaling failures were observed in the polycarbonate plates, one involves front petaling (run PL-6 for an impact angle of 37°). This is shown in Fig. 5, which is similar to the patterns exhibited in Figs 2 and 3. Another type of petaling failure, "side petaling" was observed by Wu and Goldsmith (1990), where only one crack was initiated at the upper point of the projectile/target interface that subsequently propagated outwards. Two petals were formed in front of the projectile lateral surface which were bent sideways. This type of failure is present in run PL-7 for an impact angle of 34° and is presented in Fig. 6. After perforation, the portion of the plate that deformed previously tends to return elastically to its initial position. It was also observed that the holes in the thicker polycarbonate plates were smaller than those in the thinner plates under conditions of normal perforation. Most of the polycarbonate tests occurred at or near normal incidence and the photographs of two of the three perforations at significant impact angles were obscured; hence, variations in terminal velocity, final oblique angle and crater length, obtained for the steel samples, could not be established for the plastic material.

Global target bending occurred in all tests, particularly when the initial velocity was relatively low and the impact angle relatively large. In steel targets, substantial plastic deformation was found to occur around the edge of the hole. Examination of the specimens showed that the width of the plastic zone is roughly thrice the thickness of the plates, the transverse deflection decreases with an increase of the initial velocity.

ANALYTICAL MODELING

Since the deformation patterns and failure modes of the steel targets exhibit certain similarities to those of thin aluminum targets as noted by Li and Goldsmith (1996a), the analytical model developed by them (1966b) for these samples and fully described in that reference was also utilized for the steel plates. A full description of the methods employed is presented in the (1966b) paper and also in Li (1994). The model divides the perforation process into three stages: (1) plugging; (2) hole enlargement; and (3) front petaling.

Plugging is analyzed by energy dissipation rates involving three mechanisms: (a) that involved in peripheral shear that separates the plug from the target element; (b) the energy of plastic deformation of the plug required for target and projectile attaining a common velocity and, finally; (c) that representing the energy of motion acquired by the plug. Hole enlargement, stage (2), which is usually concurrent with phase (1) except for normal perforation, involves an asymmetric stress distribution and an ovaloid hole. Equations of equilibrium, a yield criterion for an elastic/plastic target without strain hardening and the conditions of constant volume provides a relation for the thickening of the plate around the hole and the forces and moments acting on the target. Front petaling, (3), considers (a) the energy rate due to fracture, (b) the localized work in a shear zone contiguous to the

Fig. 2. Impact and distal sides, (a) and (b), of a 1.6 mm thick 4130 steel plate after perforation by a tumbling projectile, run ST-14. Initial velocity: 570 m s^{-1}; impact angle: 13°; initial oblique angle: 8°.

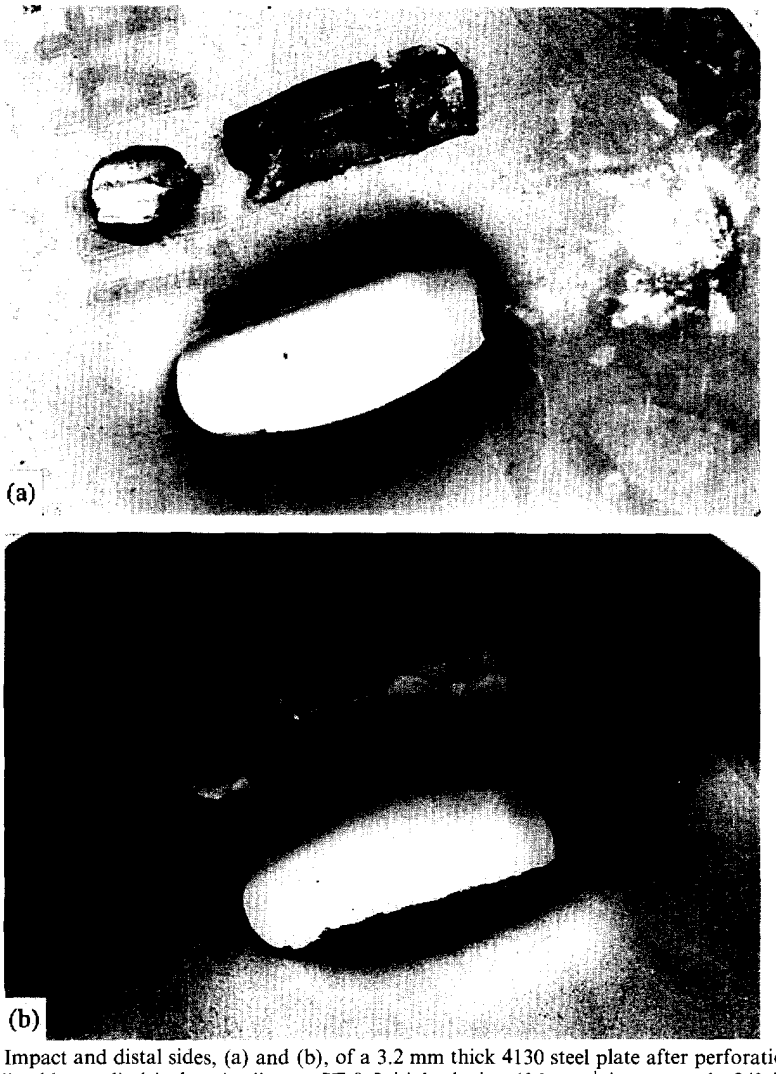

Fig. 3. Impact and distal sides, (a) and (b), of a 3.2 mm thick 4130 steel plate after perforation by a tumbling blunt cylindrical projectile, run ST-8. Initial velocity: 436 m s^{-1}; impact angle: 34°; initial oblique angle: 8°.

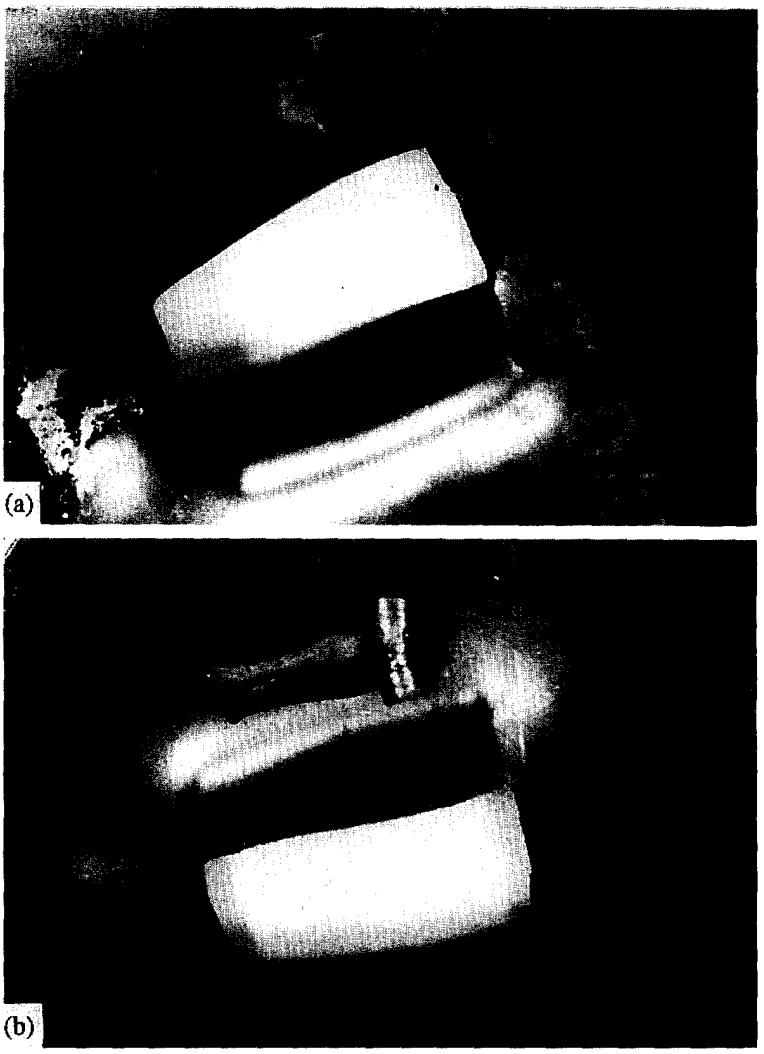

Fig. 4. Impact and distal sides, (a) and (b), of a 1.6 mm thick 4130 steel plate after perforation by a tumbling blunt cylindrical projectile, run ST-15. Initial velocity: 300 m s^{-1}; impact angle: 61°; initial oblique angle: 17°.

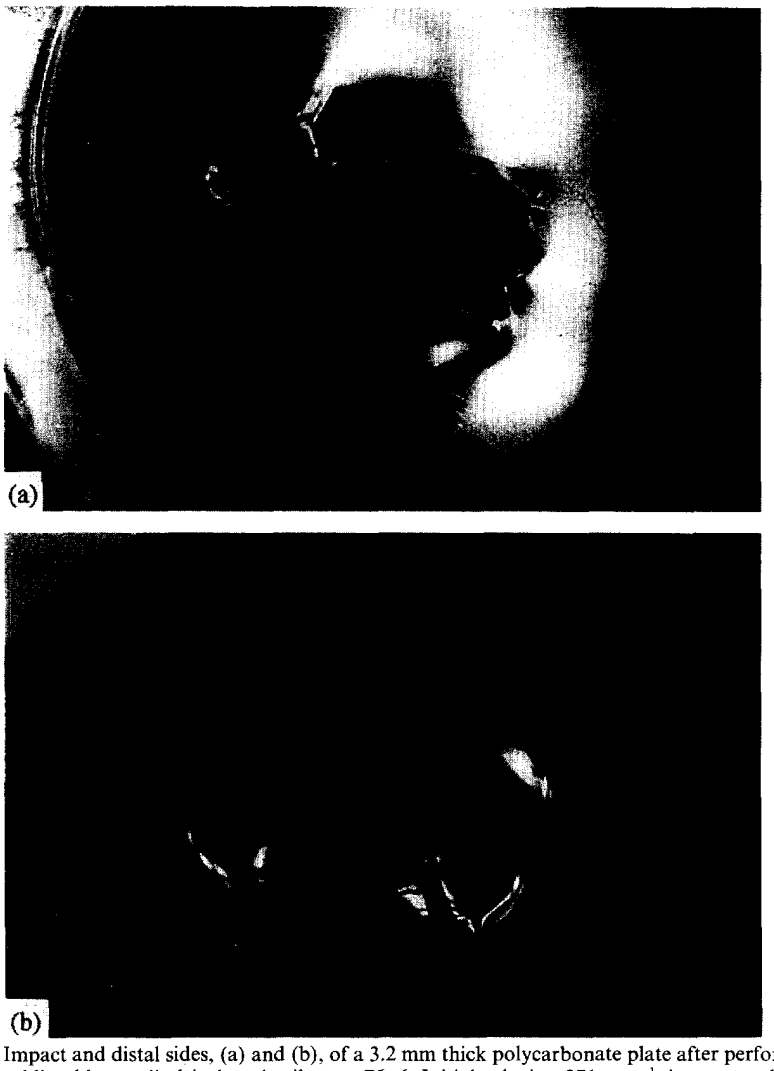

Fig. 5. Impact and distal sides, (a) and (b), of a 3.2 mm thick polycarbonate plate after perforation by a tumbling blunt cylindrical projectile, run PL-6. Initial velocity: 271 m s^{-1}; impact angle 37°; initial oblique angle: 12°.

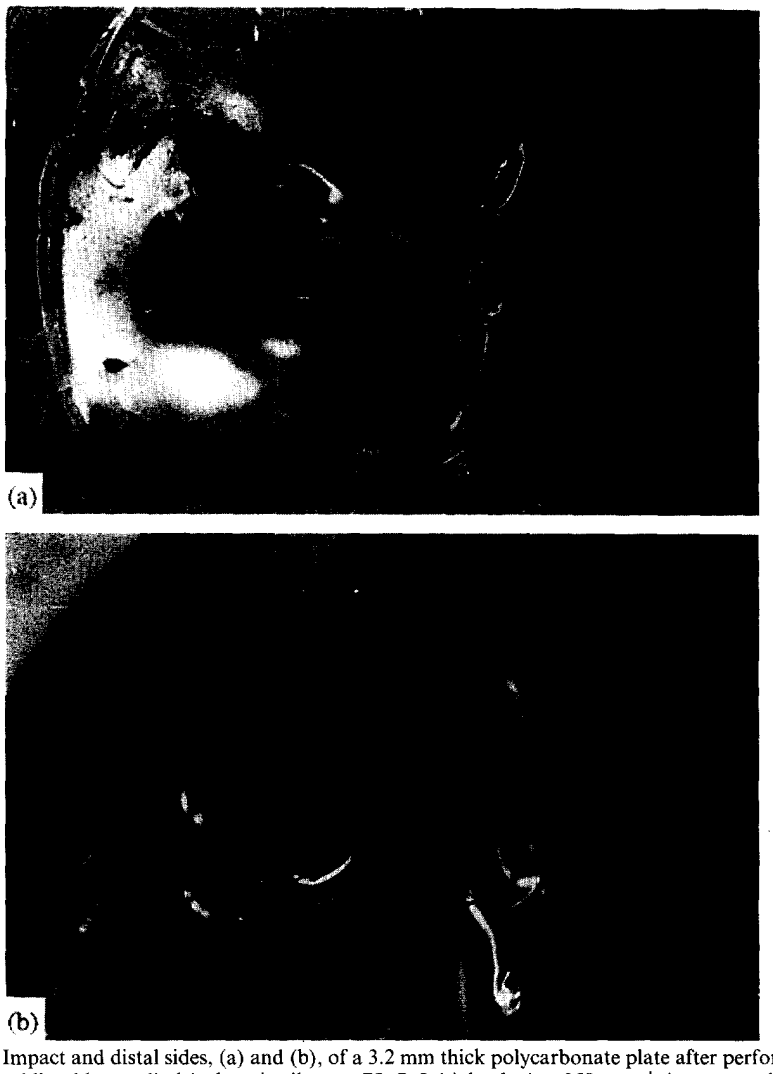

Fig. 6. Impact and distal sides, (a) and (b), of a 3.2 mm thick polycarbonate plate after perforation by a tumbling blunt cylindrical projectile, run PL-7. Initial velocity: 259 m s^{-1}; impact angle 34°; initial oblique angle: 14°.

torn edge, (c) the kinetic energy and (d) the bending energy of the petal, relating the energy rates to the work done by the forces and moments acting on the striker. When combined with the equations of motion of the rigid projectile, the various combined mechanisms can be evaluated numerically. Stage (3) eventuates only when there is a transition from hole enlargement to petaling.

Analytical and experimental results for 15 runs on 4130 steel, compared in Table 3, are in good correspondence. Figure 7 depicts their comparison for the percentage velocity drop, $100\ (v_o - v_f)/v_o$, and Fig. 8 shows the variation of the crater length, both as a function of impact angle for 3.2 mm thick 4130 steel plates struck by a blunt-faced projectile at 450 m s^{-1} for an impact angle $\Theta = 8°$. Both velocity drop and crater length increase with impact angle up to 50°, the latter much more rapidly than the former. The effect of the impact angle on the trajectory is also substantial; it reduces the oblique angle when the impact angle is low. However, the decrease becomes smaller when the impact angle exceeds 20° and tends to zero beyond 50°, suggesting a stable condition of side-on impact. A similar phenomenon was observed by Li and Goldsmith (1996a) in thin aluminum plates. Substantial discrepancies between predictions and test results in some cases may be attributed to errors in the reading of the film and to some scatter of the data.

NUMERICAL SIMULATION

Numerical simulation of perforation of run ST-3 using the non-linear three-dimensional finite element code DYNA-3D as documented by Whirley and Hallquist (1991) are

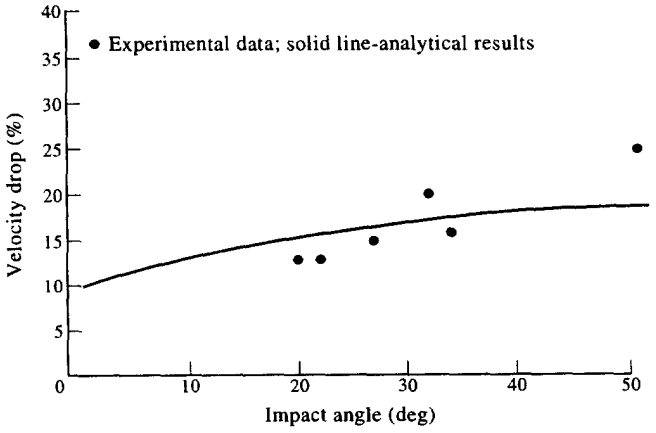

Fig. 7. Experimental and analytical results of the percentage velocity drop, $110 \times (v_o - v_f)/v_o$, as a function of impact angle for 3.2 mm thick 4130 steel plates struck by blunt cylindrical projectile. Initial oblique angle: 8°; ○: experimental data; solid line: analytical results.

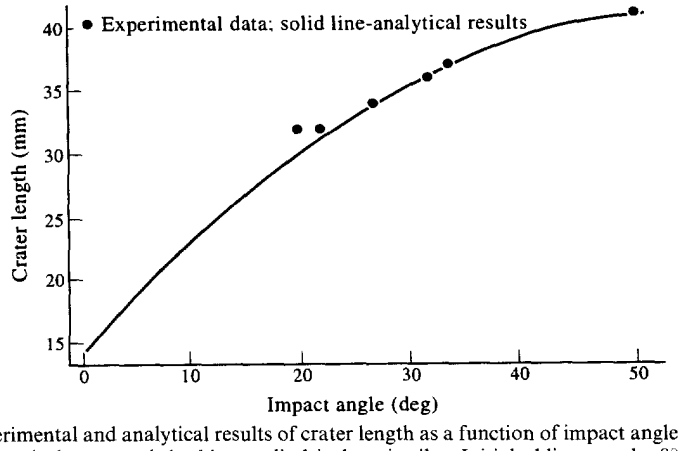

Fig. 8. Experimental and analytical results of crater length as a function of impact angle for 3.2 mm thick 4130 steel plates struck by blunt cylindrical projectiles. Initial oblique angle: 8°; ○: experimental data; solid line: analytical results.

Table 3. Experimental and analytical results of perforation of plates by tumbling cylindrical projectiles

		Initial conditions				Final results							
Run	Target thickness (mm)	Velocity ($m\ s^{-1}$)	Impact angle (deg)	Oblique angle (deg)	Angular velocity ($rad\ s^{-1}$)	Velocity[e] ($m\ s^{-1}$)	Velocity[a] ($m\ s^{-1}$)	Oblique angle[e] (deg)	Oblique angle[a] (deg)	Angular velocity[e] ($rad\ s^{-1}$)	Angular velocity[a] ($rad\ s^{-1}$)	Crater length[e] (mm)	Crater length[a] (mm)
ST-2	3.2	427	20	8	986	371	364	−1	2	912	1149	34	32
ST-3	3.2	459	22	7	1031	400	395	−1	2	1017	1186	33	32
ST-4	3.2	365	40	10	1679	282	284	5	4	2100	2176	42	39
ST-6	3.2	461	32	8	1615	368	388	3	3	1617	1810	37	36
ST-7	3.2	482	27	7	1313	410	414	−1	2	1152	1454	35	34
ST-8	3.2	436	34	8	1596	367	361	1	3	1655	1855	39	37
ST-9	3.2	418	51	10	2754	314	334	9	8	2558	3036	41	41
ST-10	3.2	703	0	0	0	650	647	0	0	0	0	14	13
ST-11	3.2	570	0	0	0	526	524	0	0	0	0	14	13
ST-12	1.6	627	14	3	1873	581	598	2	2	1926	1813	27	25
ST-13	1.6	554	16	5	1494	498	527	1	4	623	1471	28	28
ST-14	1.6	570	13	4	819	537	544	1	3	2310	831	25	24
ST-15	1.6	300	63	17	3012	264	265	16	18	3104	3570	40	40
ST-16	1.6	686	0	0	0	655	658	0	0	0	0	14	13
ST-17	1.6	556	0	0	0	530	532	0	0	0	0	14	13

Superscript: e—experimental results; a—analytical results.

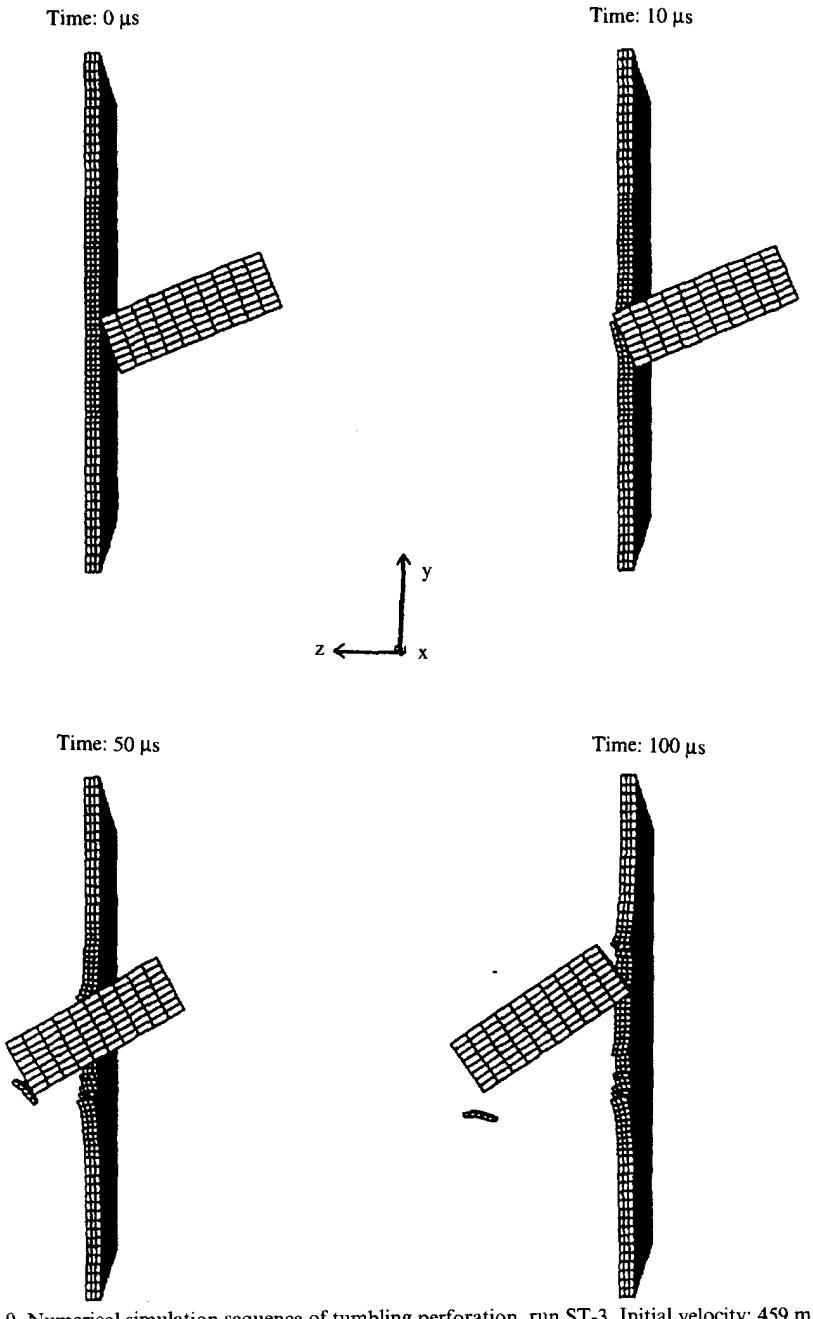

Fig. 9. Numerical simulation sequence of tumbling perforation, run ST-3. Initial velocity: 459 m s^{-1}; impact angle: 22°C; initial oblique angle: 7°.

Table 4. Experimental, analytical and numerical results for run ST-3

	Final velocity, ms^{-1}	Final oblique angle,	Crater length, mm
Experimental	400	−1	33
Analytical	395	2	32
Numerical	388	2	33

shown in Fig. 9. An elasto-plastic material model was considered for the targets with the failure criterion based on the ultimate tensile strain, while the projectile was treated as undeformable. The slide surface SAND was employed to simulate the perforation process involving failures such as plugging and petaling yielding final velocity and obliquity. The final angle of the projectile as well as the crater length of the target predicted by the numerical simulation, the experimental study and the analytical modeling are presented in Table 4.

The correlation between the three sets of results is very good. Failure of the target due to tumbling consists primarily of two modes: plugging and front petaling. Both of these stages were observed in the experiments by Li and Goldsmith (1966a) and assumed by them (1966b) in the analytical model for the thin targets. The translational velocity and trajectory histories from the analytical modeling and the numerical simulation is portrayed in Fig. 10. Again, good correlation of the detailed perforation process was found between these results. The two figures show two distinct stages in the perforation process: the first stage, plugging, lasts from 0 to 15 to μs, while the second, petaling, occurs from 15 to 82 μs. The velocity drop is large in the plugging stage and decrease during petaling. Even though the time for plugging is short, most of the kinetic energy of the projectile is consumed in this stage. The trajectory change of the projectile occurred mainly during the petaling phase.

CONCLUSIONS

An experimental study of the effect of tumbling of blunt cylindrical projectiles on the impact response of thin steel and polycarbonate plates was executed; various failure modes were observed and discussed. Impact on steel targets show effects similar to those observed in thin aluminum plates. The analytical model developed for the latter case was also employed for the steel target and a numerical simulation of a single run was performed. Comparisons among the experimental, analytical and numerical results show excellent agreement not only for the final velocity and oblique angle, but also for the detailed perforation process as indicated by the velocity and trajectory histories of the projectile.

It was found that an increase of the impact angle can increase the velocity drop and crater length as well as change the trajectory of the projectile considerably. However, the effect tends to be stabilized when the impact angle is greater than 50° and this case is similar to side-on impact for the ranges of velocity and target thickness investigated here. This conclusion is important in spaced armor design. To achieve maximum protection from projectile penetration, a high impact angle, which results in a velocity drop increase, is desirable. Since a 50° impact angle has the same effect as a 90° angle, the achievement of a 50° angle for a tumbling projectile requires only about half the travel distance required by a 90° impact angle, so that half of the space between the armors can be saved by a choice of a 50° impact angle.

Acknowledgements—This work constitutes a portion of a doctoral dissertation by the first author at the University of California, Berkeley. This investigation was sponsored by the Air Force Office of Scientific Research, Bolling Air Force Base, Washington, D. C., under contract AFOSR F49620-89-8127. The authors express their appreciation to Lawrence Livermore National Laboratory for providing the DYNA-3D code and to the Supercomputing Centers at Pittsburgh and San Diego for the execution of the simulations.

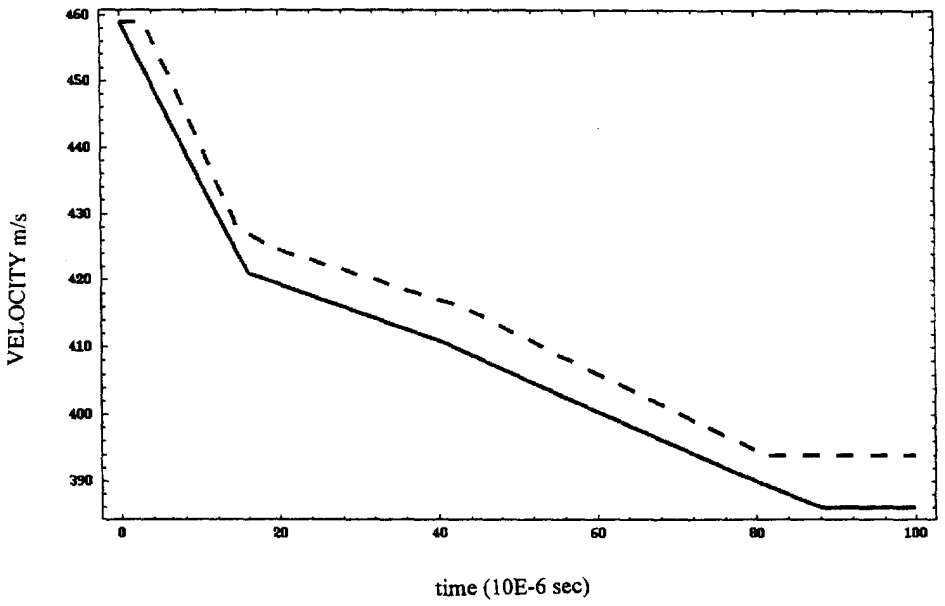

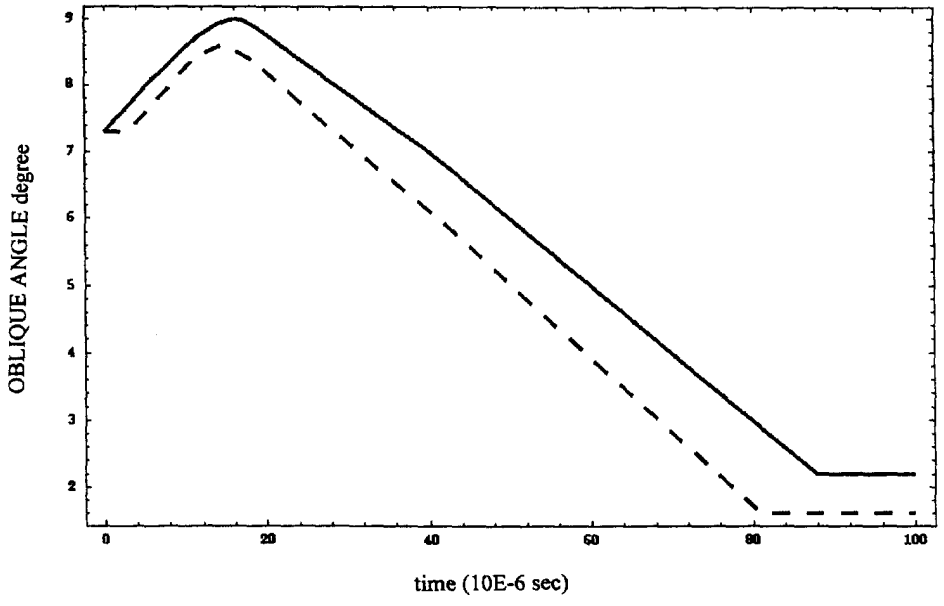

Fig. 10. Comparison of velocity histories of the center of a tumbling projectile and the oblique angle obtained by analytical modeling and numerical simulation, run ST-3. Initial velocity: 459 m s^{-1}; impact angle: 22°; initial oblique angle: 7°. Dashed line: analytical solution; solid line: numerical solution.

REFERENCES

Li, K. (1994). Effect of Tumbling of Cylindrical Projectiles on the Impact Response of Target Plates. Ph.D. dissertation, University of California, Berkeley.

Li, K. and Goldsmith, W. (1995). Numerical simulation of perforation of aluminum plates by tumbling projectiles. In: *Constitutive Laws: Experiment and Numerical Implementation*, ed. A. M. Rajendran and R. C. Batra, pp. 268–280. Barcelona, Spain.

Li, K. and Goldsmith, W. (1996a). Impact on aluminum plates by tumbling projectiles: experimental study. *International Journal of Impact Engineering*, **18**, 23–43.

Li, K. and Goldsmith, W. (1996b). An analytical model for tumbling projectile perforation of thin aluminum plates. *International Journal of Impact Engineering*, **18**, 43–56.

Li, K and Goldsmith, W. (1996c). A phenomenological model for perforation of moderately thick plates by tumbling projectiles. *International Journal of Solids & Structures*, **33**, 3561–3575.

Metals Handbook: *Properties and Selections* (1978), 9th edn. American Society for Metals, Philadelphia, PA.

Whirley, R. G. and Hallquist, J. O. (1991) DYNA-3D, a nonlinear, explicit three-dimensional finite element code for solid and structural mechanics—user's manual. University of California, Lawrence Livermore National Laboratory, UCRL-MA-107245.

Wu, E. and Goldsmith, W. (1990) Normal impact of blunt projectiles on moving targets: experimental study. *International Journal of Impact Engineering*, **9**, 389–404.